J.Natn.Sci.Foundation Sri Lanka 2022 50 (3): 625 - 637
DOI: http://dx.doi.org/10.4038/jnsfsr.v50i3.10593

RESEARCH ARTICLE

Manufacturing and Industrial Engineering

Failure prediction of solid resilient tyres due to kerb impact: A finite element modelling approach

WAAS Premarathna[1*], JASC Jayasinghe[2], CD Senanayake[1], KK Wijesundara[2] and P Gamage[1]

[1]*Department of Manufactury and Industrial Engineering, Faculty of Engineering, University of Peradeniya, Peradeniya.*
[2]*Department of Civil Engieneering, Faculty of Engineering, University of Peradeniya, Peradeniya.*

Submitted: 21 June 2021; Revised: 25 May 2022; Accepted: 24 June 2022

Abstract: Solid resilient tyres frequently impact on kerbs or obstacles when they are operated in the construction and transportation sectors. These sudden impacts can generate high stresses and thereby damage the tyre. The factors which cause such failures are not easy to capture experimentally due to their complexity and high experimental cost. Hence, this study focused on using the finite element method to model the solid resilient tyre, generate stresses, and identify the failures and regions that are susceptible to damage. Initially, a tyre static model was developed and validated using laboratory experimental data obtained from the industry. The validation results showed that the numerical results are in good agreement with the experimental data. Subsequently, the model was extended to incorporate impact simulation. The simulation considered tyre motion and impact on three different types of kerbs - angular, circular and square-shaped. Simulation results showed that high stresses occur mainly in the side walls of the solid tyre while high contact pressure and high in-plane shear stresses were observed at the tread layer especially when it moves on square-type kerbs. Hence, there is a high tendency for tyre failures to occur due to the side wall cracks at the base layer. Furthermore, sudden wear and damage due to chunking can be expected on the tread layer of the solid resilient tyre.

Keywords: Hyper-elastic models, impact simulations, non-linear finite element model, solid resilient tyres.

INTRODUCTION

Solid resilient tyres are mainly utilized in forklift vehicles and often operate in harsh environmental conditions while bearing heavy loads. In these rugged environmental conditions, the tyres experience high stresses, which may lead to sudden wearing and damage due to chunking and rupturing that occur when the tyre impacts on kerbs or obstacles. High experimental cost and time are the main impediments to investigating such behaviour of solid tyres using experimental setups. In this study, finite element (FE) numerical modelling approaches have been utilized to model and predict the solid tyre impact behaviour. The main components of solid resilient tyres and their functions are illustrated in Figure 1. The base layer and embedded bead bundles of the solid tyre ensure good gripping contact with the tyre rim. The internal heat generation and traction of the tyre mainly occur in the cushion layer and tread layer, respectively.

Most of the literature has focused on the numerical analyses of pneumatic tyres (Han *et al.*, 2019; Azizi, 2020). Even for those analyses, the impact analyses were performed for rectangular cleats or kerbs only. Wei and Olatunbosun (2014) studied the impact analysis of a pneumatic tyre and their findings showed that when the height of the rectangular obstacles was increased the amplitude of the vertical force and longitudinal force on the tyre and the tyre deformation were also increased. Suvanjumrat and Rugsaj (2020) investigated impact force and vertical deformation of non-pneumatic tyres when impacted on rectangular cleats with three different heights. Moreover, impact forces on the axle of a pneumatic tyre against a rectangular kerb were analysed by including the suspension system with a full

* Corresponding author (asaranga225@gmail.com; https://orcid.org/0000-0002-5336-2932)

car model (Shiraishi *et al.* 2000). Furthermore, Reida *et al.* (2007) used a detailed truck numerical model to study the pneumatic tyre impacts on a rectangular kerb as well as its behaviour when it was moving over rocks and culvert grates. Kamoulakos and Kao (1998) analysed the similarities of numerical and experimental readings on vertical and horizontal spindle forces when a pneumatic tyre moved over a rectangular cleat. In Chang and Yang (2009), the generation of ductile fractures on a wheel has been observed numerically as well as experimentally, by impacting it on a solid rectangular cube. Their results showed that the damage to the wheel could be accurately predicted using maximum strain energy density based on the plastic work due to the impact. Duni *et al.* (2008) reported the contact pressure behaviour of a complete car numerical model with pneumatic tyres when it was moving on a pothole and fatigue reference track. Han *et al.* (2019) conducted a transient dynamic analysis to study the pneumatic tyre behaviour when it impacted on a rectangular cleat. The results showed that large contact pressure accumulated in the two edges of the tread layer where it made contact with the road. In a more recent study of Han *et al.* (2020), they utilized a quarter vehicle model with pneumatic tyres to investigate the structural vibration and acoustic radiation under rectangular cleat impact excitations. They observed localized contact pressure on the cleat impact area, and widely distributed contact pressure around the contact region in the tyre when the tyre was on the cleat and just before it passed through the cleat. In Azizi (2020), a cleat impact experimental test was performed by using a pneumatic tyre and test drum. In this study, the frequency spectrum of the cleat impact was obtained as a function of tyre contact patch length, cleat size, and rolling speed.

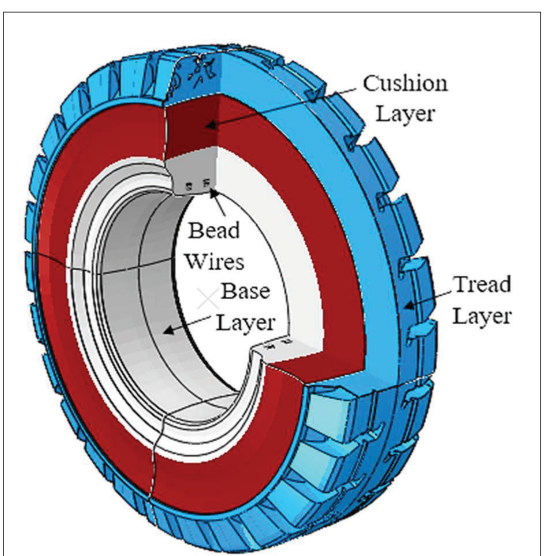

Figure 1: Components of solid resilient tyre

Few studies have been performed to analyse static and dynamic behaviours of solid resilient tyres. Suripa and Chaikittiratana (2008), investigated the strain energy density and stress distribution of solid tyres under static conditions by using simplified 3D FE solid models. The results showed that the highest strain energy accumulated in the cushion layer of the solid tyre. Dechwayukul *et al.* (2010) also conducted laboratory tests to analyse solid tyre durability to evaluate tyre service life. Phromjan and Suvanjumrat (2018a) presented the development of a detailed 3D FE model to analyse the deformations and stress distributions of a solid tyre under different load levels in static conditions. In their results, high stress was observed in the base layer of the solid tyre. Phromjan & Suvanjumrat (2018b) conducted lab experiments to compare the contact forces and vibration analyses of a rolling solid tyre and a pneumatic tyre under different rolling velocities. It was identified that higher contact forces and vibration levels were generated in solid tyres than in pneumatic tyres. To the best of the authors' knowledge, there have been no dynamic numerical FE models developed to study the impact of solid resilient tyres on kerbs and predict their failures.

The structure of this paper is as follows: In the methodology section, the development procedures for static and impact models of a solid resilient tyre are presented. The next section presents the model validation, analysis of results, and discussion. The final section provides concluding remarks and possible future research directions.

MATERIALS AND METHODS

3D FE model of the solid tyre

A CAD model of a solid resilient tyre was first developed as shown in Figure 2. A detailed numerical model of the solid resilient tyre was then developed for the static analysis using Abaqus 6.14 software (ABAQUS Inc., 2014) and the procedure is shown in Figure 3.

In the detailed numerical model, the tyre constraints were applied on nodes which were in between the three rubber layers. Surface-to-surface contact was incorporated to assign interactions between contact surface and tread layer of the tyre. A mesh convergence analysis was performed to identify the suitable mesh size of the tyre, as shown in Figure 4. The mesh of all components in the tyre was modelled by using 8-node 3D hexahedral elements and the converged model contains in total 71685 solid elements. The inner surface of the base layer was assigned as a rigid body to represent the tyre rim. Loads were applied to the centre of the tyre.

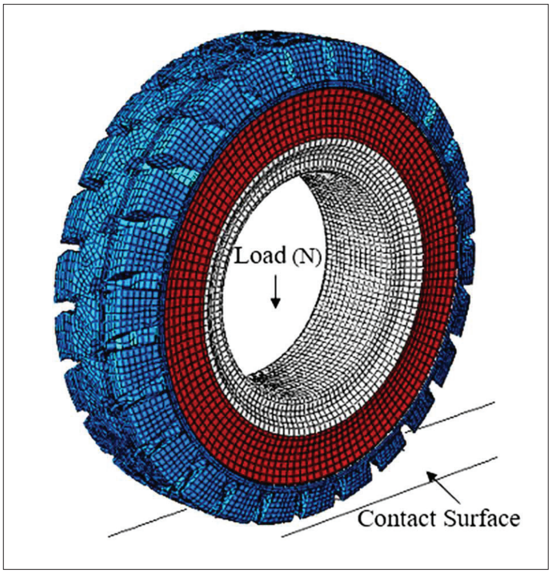

Figure 2: Static numerical model of solid resilient tyre

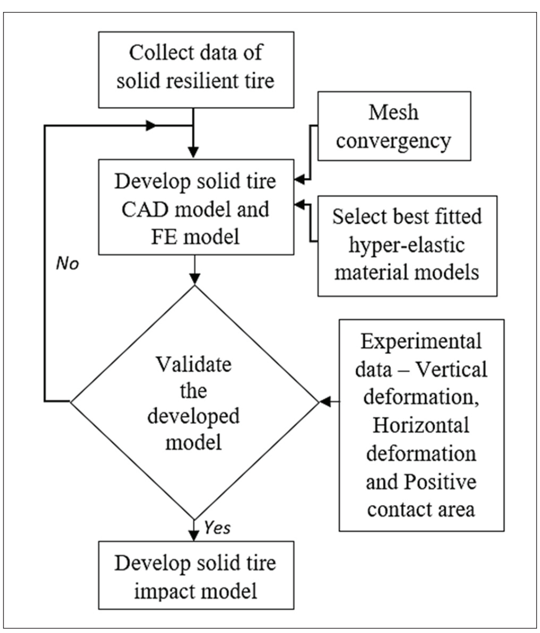

Figure 3: Methodology flow chart of static FE model development

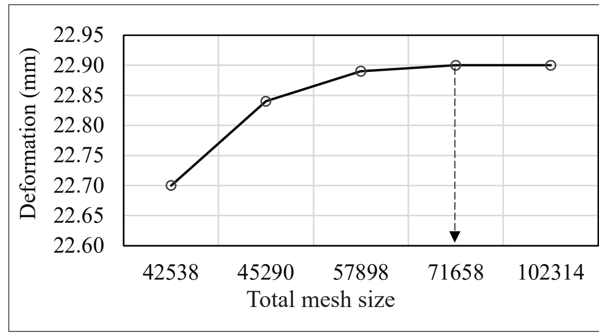

Figure 4: Mesh convergence with vertical deformation

Selection of best-fitted hyper-elastic material models

Suitable hyper-elastic material models are required to develop the static model of the solid tyre. The best-fitted material models are utilized to describe the mechanical behaviour of rubber layers in the solid tyre. In this study, the best-fitted material models for base layer, cushion layer, and tread layer were selected by combining the curve fitting method and three standard measures of accuracy (MAPE: Mean Absolute Percentage Error; MAD: Mean Absolute Deviation; and MSD: Mean Squared Deviation). Based on the results of curve fitting, the Mooney-Rivlin, Ogden, and Yeoh hyper-elastic material models were obtained as the best-fitted material models of the base layer, cushion layer and tread layer, respectively. Equations 1, 2, and 3 represent the general form of the Mooney-Rivlin material model, Yeoh material model, and Ogden material model, respectively (Mooney, 1940; Ogden, 1972; 1973; Yeoh, 1990; 1997).

$$U = C_{10}(\bar{I}_1 - 3) + C_{01}(\bar{I}_2 - 3) + \frac{1}{D_1}(J_{el} - 1)^2 \quad ...(1)$$

$$U = \sum_{i=0}^{3} C_{i0}(\bar{I}_1 - 3)i + \sum_{i=1}^{3} \frac{1}{D_i}(J_{el} - 1)^{2i} \quad ...(2)$$

$$U = \sum_{i=1}^{N} \frac{2\mu_i}{\alpha_i^2}(\bar{\lambda}_1^{\alpha_i} + \bar{\lambda}_2^{\alpha_i} + \bar{\lambda}_3^{\alpha_i} - 3) + \sum_{i=1}^{N} \frac{1}{D_1}(J_{el} - 1)^{2i} \quad ...(3)$$

Where:

λ_1, λ_2 and λ_3 : Principle stretches of principle directions; C_{ij} and D_{ij} : Material constants which control the shear behaviour and bulk compressibility of the material; J_{el} : Elastic volume ratio; $\bar{I}_n$: Invariants; μ_i and α_i : Temperature-dependent material coefficients

Table 1 presents the best-fitted hyper-elastic material models and their coefficient values for each rubber layer of the solid tyre.

Dynamic impact simulation of the solid tyre

The validated static numerical model of the solid resilient tyre was utilized to implement the impact numerical model of the tyre. Figure 5 illustrates the steps that were followed to develop the tyre impact model. The *Abaqus/Explicit* solver has been utilized to generate this model. The *Abaqus* results transferring capability was employed to transfer results from *Abaqus/Std*. to *Abaqus/Explicit*. Furthermore, relevant boundary conditions and velocities were also applied to the tyre model. Since solid tyres usually move short distances at low velocities, 5 kmh^{-1} and 10 kmh^{-1} translational velocities were accounted as impact velocities of the tyre model. Finally, the generation of maximum stress in the rubber layers, maximum contact pressure, and shear stress due to friction were determined at the time of tyre impacts on three types of kerbs. In these impact models, the tread layer of the tyre was ignored to avoid convergence issues and to reduce the simulation time.

The relaxation property of each rubber layer was assigned by considering the viscoelastic behaviour of the rubber material. The corresponding viscoelastic properties were obtained by utilizing the dynamic mechanical analyzer (DMA) as shown in Figure 6 and frequency sweep test data.

Table 1: Coefficients of best-fitted hyper-elastic material models for tyre base, cushion and tread layers

Rubber layer of the tyre	Base		Cushion						Tread		
Material model	Mooney-Rivlin		Ogden						Yeoh		
Coefficients	C_{10}	C_{01}	μ_1	μ_2	μ_2	α_1	α_2	α_3	C_{10}	C_{20}	C_{30}
	0.6	2.5	-9.3	8.9	0.9	1.5	2.1	-3.7	0.7	-0.1	0.1

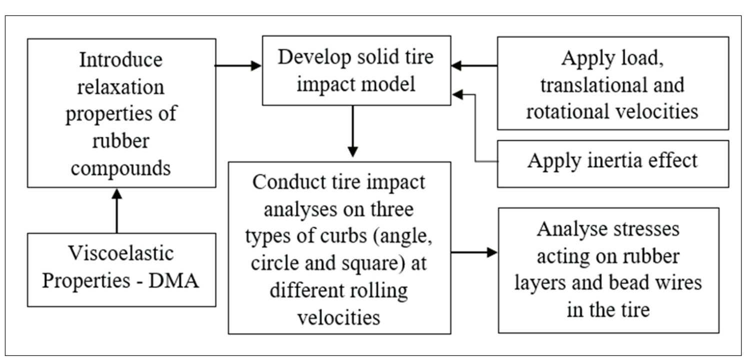

Figure 5: Flow chart of impact FE model development

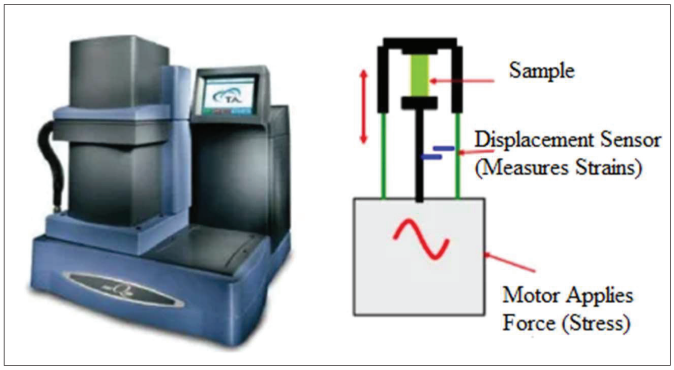

Figure 6: Dynamic mechanical analyser
(Eindhoven University of Technology, 2021)

Table 2: Coefficients of Prony series for tyre base layer, cushion layer and tread layer

Rubber layer of the tyre	Three-term Prony coefficients					
	g_1	ψ_1	g_2	ψ_2	g_3	ψ_3
Base	0.2208	0.0003	0.1208	0.0146	0.0993	0.1890
Cushion	0.0016	0.0001	0.1099	0.0173	0.0603	0.2198
Tread	0.1545	0.0032	0.1223	0.0377	0.1253	1.8288

The corresponding storage modulus (G') and loss modulus (G'') data of the rubber materials were obtained using the frequency sweep test. Equations (4) and (5) express the relationship between Prony series coefficients related to storage modulus and loss modulus of the material, respectively.

$$G'(\omega) = G_0\{[1 - \sum_{n=1}^{N} g_n] + [\sum_{n=1}^{N} \frac{g_n\omega^2\psi^2}{1+\omega^2\psi^2}]\} \quad ...(4)$$

$$G''(\omega) = G_0\{\sum_{n=1}^{N} \frac{g_n\omega\psi}{1+\omega^2\psi^2}\} \quad ...(5)$$

Where:

ω : Rolling frequency of the tyre

G_0 : Instantaneous shear modulus

g_n and ψ_n : Prony series coefficients

The obtained three-term Prony series coefficients are presented in Table 2. Subsequently, the tyre impact model was implemented using the validated static numerical model of the solid tyre as shown in Figure 7.

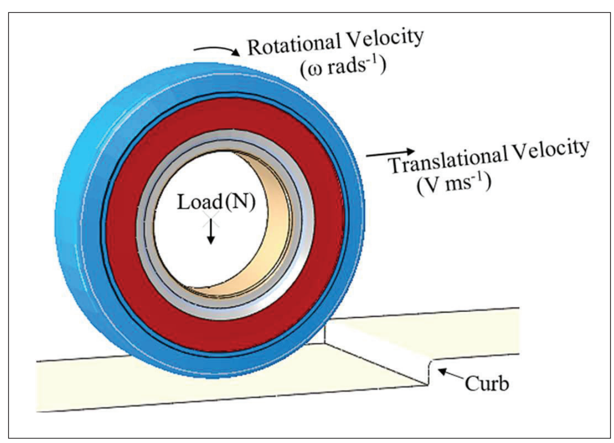

Figure 7: Impact numerical model of solid tyre

Selection of kerbs

According to the literature review, most of the impact analyses were performed for pneumatic tyres with square-type kerbs. Hence, it is necessary to select suitable kerb geometries to perform the impact analyses on solid tyres. Equal height and three different types of kerb geometries were introduced onto the contact surface as shown in Figure 8. The kerbs were selected based on their practical usage (Hills Kerbs PTY Ltd., 2021). The following kerb types are usually utilized on the edges of pavements, roads and parking areas.

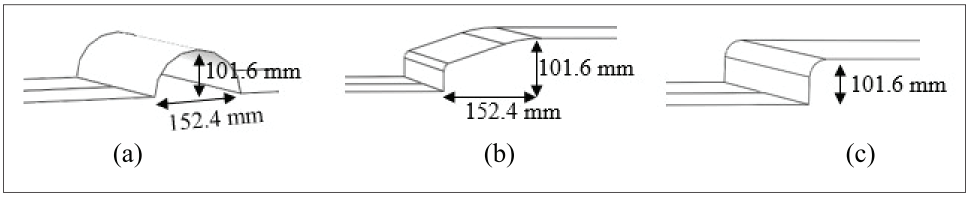

Figure 8: Three types of kerbs: (a) circular type, (b) angle type and (c) square type

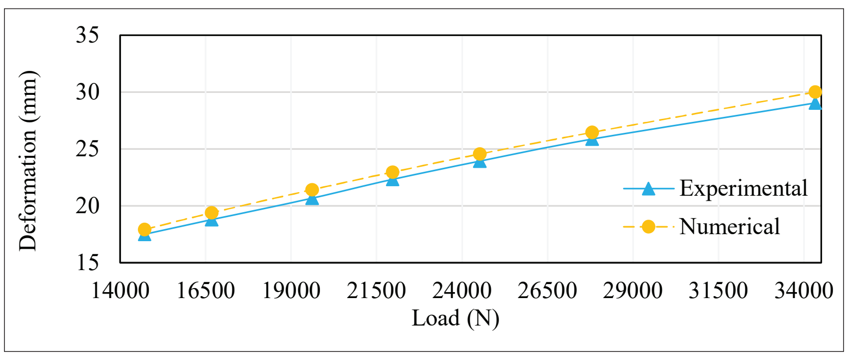

Figure 9: Experimental and numerical vertical deformation data of the solid tyre

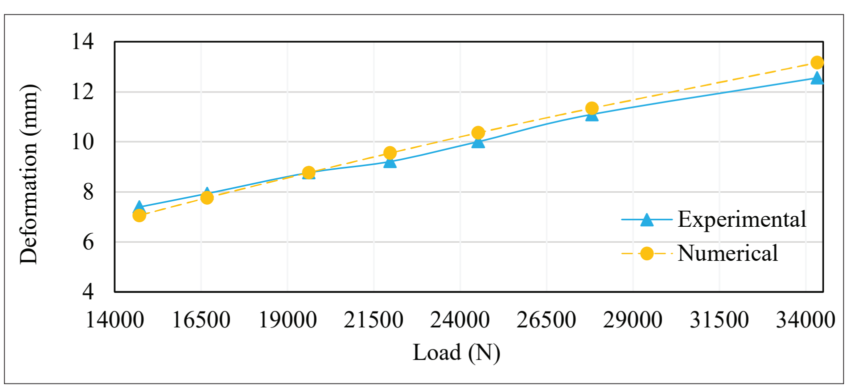

Figure 10: Experimental and numerical horizontal deformation data of the solid tyre

RESULTS AND DISCUSSION

Validation of the solid tyre numerical model

The developed static model was validated by applying different loads on it and comparing corresponding deformation readings with laboratory experimental data. Figures 9 and 10 illustrate the vertical and horizontal deformations of the numerical tyre model and actual tyre.

Table 3: Readings of three measures of accuracy

Type of the deformation	MAPE (%)	MAD (%)	MSD (%)
Vertical	2.91	0.66	0.46
Horizontal	3.00	0.29	0.12

Table 3 shows the values of three measures of accuracies calculated between experimental and numerical results. According to the Table 3 results, the Mean Absolute Percentage Error (MAPE) value for vertical and horizontal deformations are 2.19% and 3.00%, respectively. The readings of Mean Absolute Deviation (MAD) and Mean Squared Deviation (MSD) also show very small values (<1%). Hence, the values of the three measures of accuracy results confirmed that the behaviour of the developed tyre model is in good agreement with the actual tyre behaviour.

Analysis of maximum stress generation on the solid tyre during the impacts

The maximum von Mises stress accumulation in the rubber components of the solid tyre under angle type, circle type, and square type kerb geometries is illustrated in Figures 11, 12, and 13, respectively. According to Figure 11, a maximum von Mises stress reading of 2.915 MPa was observed in the side wall rubber compound of the solid tyre when the tyre impacted on an angle-type kerb.

Furthermore, according to Figure 12, a maximum von Mises stress value of 2.861 MPa is detected in the side walls of the solid tyre when it impacted on a circle-type kerb.

Moreover, a maximum von Mises stress reading of 3.089 MPa is obtained in the side walls of the solid tyre when it impacted on a square type kerb, as shown in Figure 13.

Among these three types of kerbs, the solid tyre experiences a higher impact stress on the square-type kerb than on the other two kerb types. However, during the impact the fillet radius on the square-type kerb can significantly affect the generation of maximum stress in a solid tyre. Figures 14 and 15 illustrate the variation of maximum impact stress in the solid resilient tyre with 5 kmh^{-1} and 10 kmh^{-1} impact velocities, respectively. Figures 14 and 15 show that impact with the square-type kerb has resulted in a higher value of the maximum stress compared with angle and circle-type kerbs under both impact velocities.

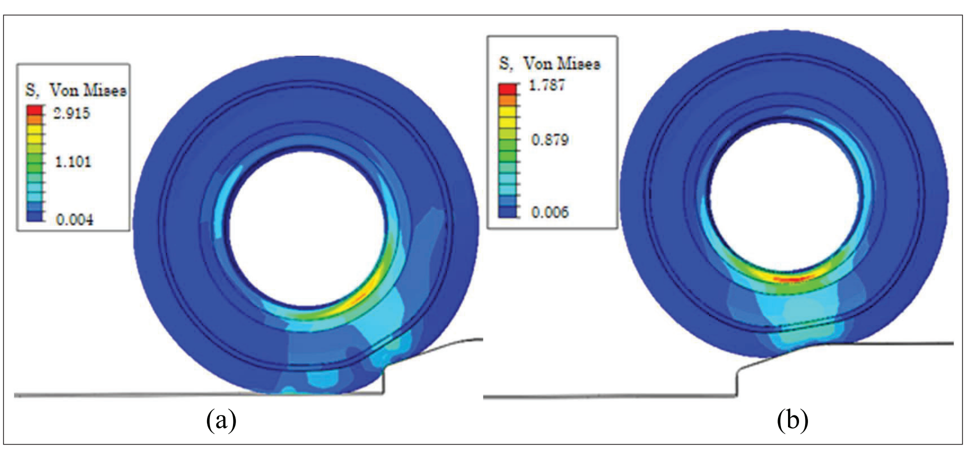

Figure 11: Stress generation of the solid tyre when it impacted on an angle type kerb (load 19614 N and velocity 10 kmh^{-1})

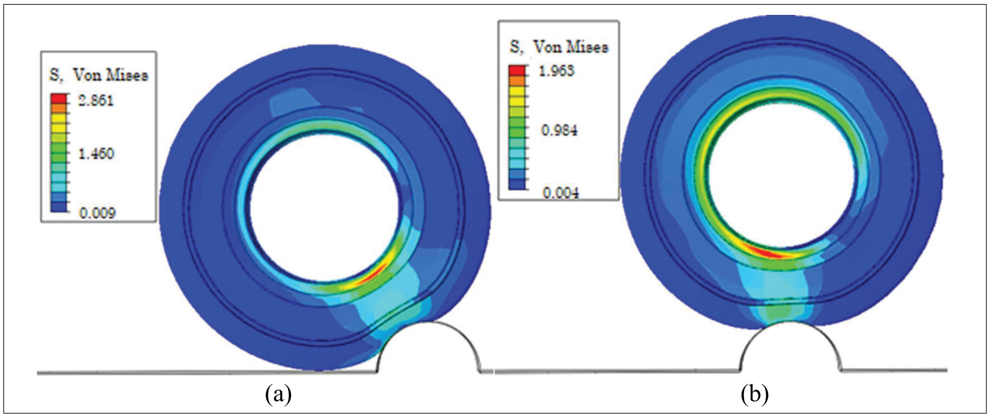

Figure 12: Stress generation of the solid tyre when it impacted on a circle type kerb (load 19614 N and velocity 10 kmh^{-1})

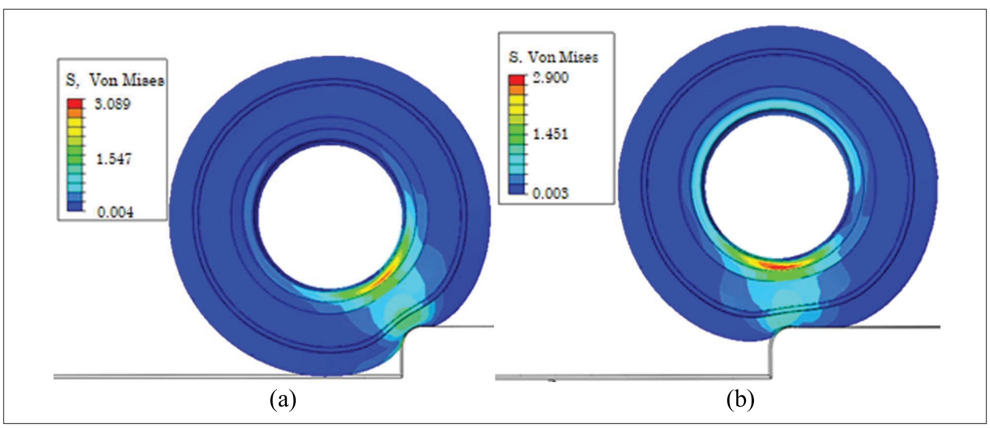

Figure 13: Stress generation of the solid tyre when it impacted on a square type kerb (load 19614 N and velocity 10 kmh^{-1})

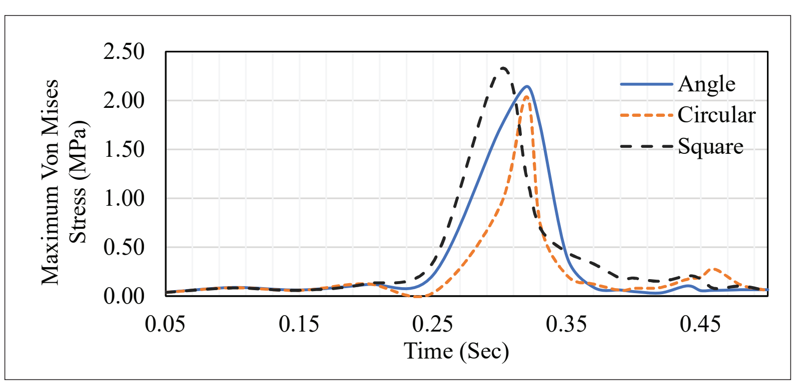

Figure 14: Maximum impact stress history of solid tyre rubber components with 5 kmh^{-1} velocity

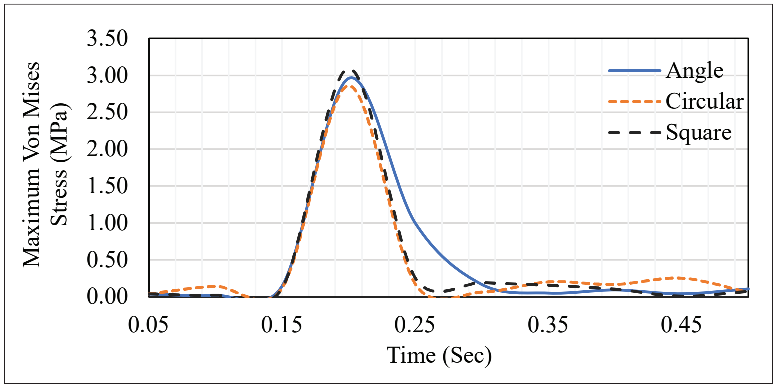

Figure 15: Maximum impact stress history of solid tyre rubber components with 10 kmh^{-1} velocity

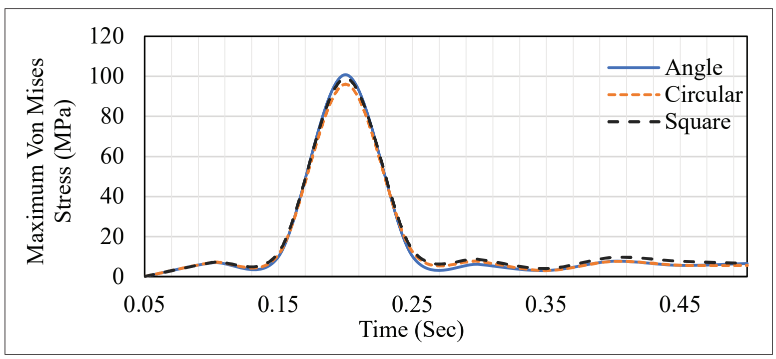

Figure 16: Maximum impact stress history of bead wires at velocity 10 kmh^{-1}

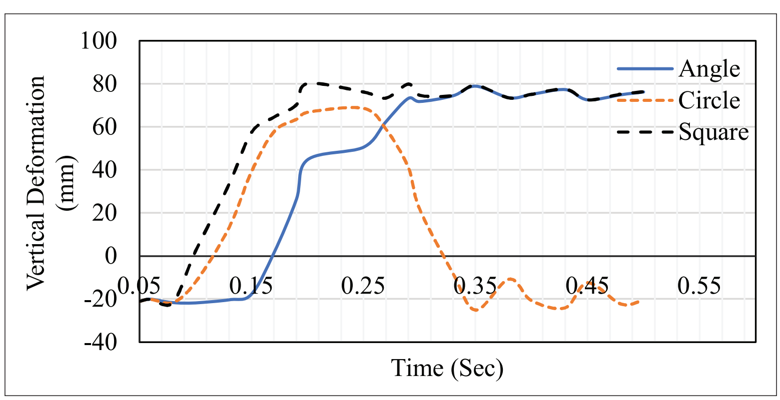

Figure 17: Deformation history of solid tyre at velocity 10 kmh^{-1}

Furthermore, it can be observed that the maximum value of the impact stress is increasing with increasing impact velocity. According to the above stress analyses, it can be seen that the high impact stresses lead to sidewall crack propagations in the solid tyre rubber components. Figure 16 illustrates the maximum stresses obtained in the bead wires of the tyre when it travels over the three types of kerbs. It is noticed that there is no significant difference among three maximum stresses generated in the bead wires based on the three types of kerbs. In addition, their peak stress values are well below the material yield stress (1765 MPa) of the bead wires.

The vertical deformations of the solid tyre for the three types of kerbs are presented in Figure 17. In the dynamic condition of the tyre, the maximum vertical deformations that can be observed are 80.1 mm for the square type kerb, 79.2 mm for the angle type kerb, and 68.6 mm for the circular type kerb. At 0.25 seconds, the tyre experiences the highest vertical deformation (80.1 mm) when it is moving over the square-type kerb.

Analysis of contact pressure generation of the solid tyre

In this section, the contact pressure of the solid tyre is examined to investigate its effect on tyre wear and tread layer damage during impact with the three different kerbs types, as shown in Figure 18.

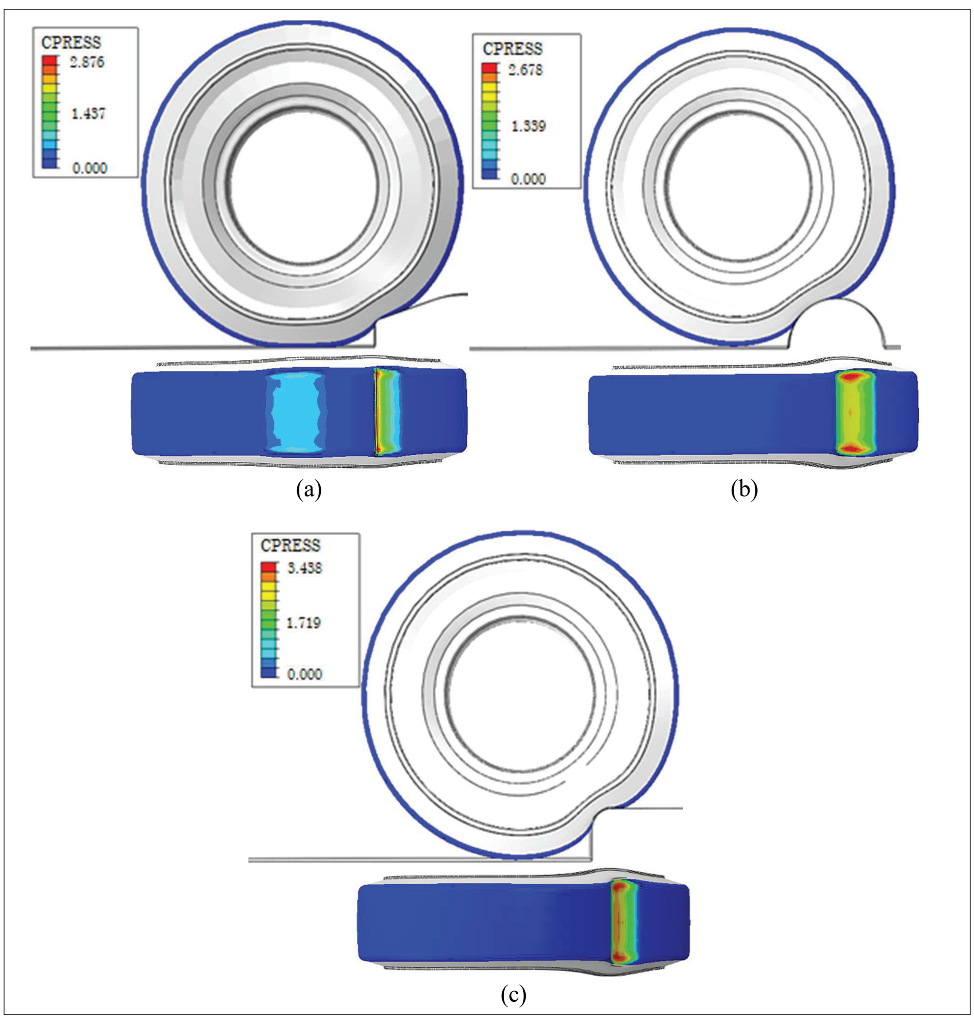

Figure 18: Solid tyre contact pressure (CPRESS in Nmm^{-2}) generation (load 19614 N and velocity 10 kmh^{-1}): (a) impact on angle type kerb; (b) impact on circle type kerb and (c) impact on square type kerb

According to the contact pressure analysis, the highest contact pressure (3.438 Nmm^{-2}) is observed when the tyre impacts on the square type kerb. Furthermore, the distribution of the contact pressure throughout the tyre contact patch varies with the type of impact kerb. Based on the contact pressure analysis, the highest wear rate and damage on tread layer can be expected from the tyre when it impacts on the square type kerb compared to the other two types of kerb. In the circle type kerb, damage in the tyre tread layer occurs closer to the edges of the tyre contact patch than the middle.

Analysis of in-plane shear stress generation of the solid tyre

The in-plane shear stress generation in the tyre circumferential direction is presented in Figure 19.

According to Figure 19, high in-plane shear stress (1.297 MPa and 1.314 MPa) is observed when the tyre impacts on the circular type and square type kerbs, respectively. This leads to sudden wear and damage due to chunking in the region of the tread layer. Based on

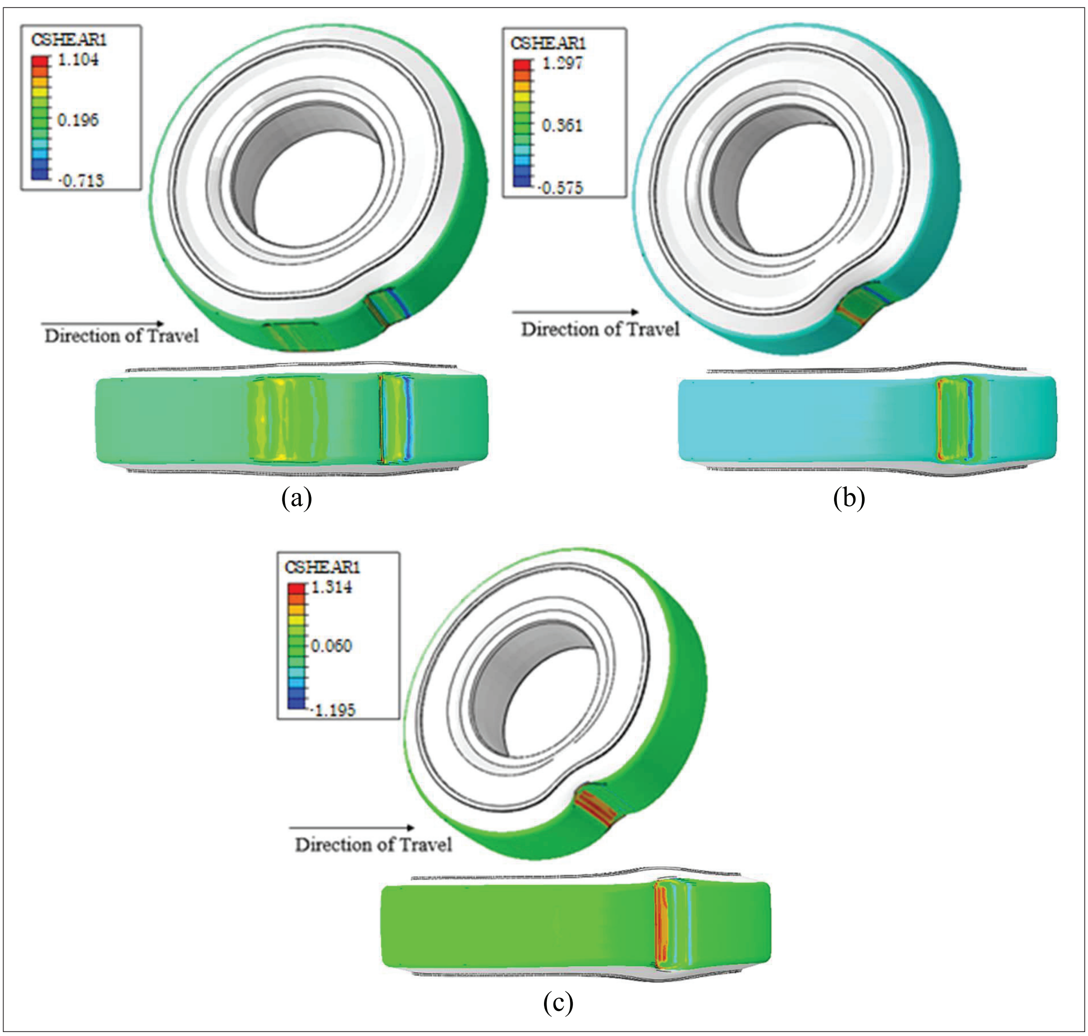

Figure 19: In plane shear stress (CSHEAR1 in MPa) generation at tread layer of the solid tyre (load - 19614 N and velocity - 10 kmh^{-1}): (a) impact on angle type kerb; (b) impact on circle type kerb and (c) impact on square type kerb

above stress analyses and contact pressure analyses, it is clear that the sudden impacts of the solid tyre on square-type kerbs have a relatively more adverse effect on the durability of the tyre.

CONCLUSIONS

This study was conducted to investigate the stress generation and failure regions of solid resilient tyres as they moved on angle, circle and square-type kerbs. The analyses were performed on stress histories, contact pressure and in plane shear stress generation of tyre rubber layers and side walls, under two different moving velocities. To obtain the behaviour of tyre impact stress histories, a validated numerical model of a tyre was developed. The numerical model was used for tyre impact analyses on the three different kerbs by importing static results into the *Abaqus*/*Explicit* interface. Based on the tyre impact analyses results, relatively higher stresses were observed in the tyre sidewalls (3.089 MPa) when it impacted on square type kerbs. The results show that there is a high tendency for the solid tyres to fail due to side wall crack propagation when the tyre moves on square-type kerbs. Furthermore, high contact pressure (3.438 Nmm^{-2}) and high in-plane shear stress (1.314 MPa) were observed at the tread layer of the tyre when it moved on a square-type kerb. These findings highlighted that impact of solid tyres with square-type kerbs can significantly decrease the service life and durability of solid tyres compared to other kerb types. Therefore, this model can be reliably used to identify and analyse improvements to the solid tyre design in order to reduce the probability of failure due to kerb impact. This study can be further extended to observe the rolling resistance and heat generation of the solid resilient tyre as well as the behaviour of tyre impact due to changes of material properties and geometry parameters.

Acknowledgement

The authors would like to thank Elastomeric Engineering Company Ltd., Horana, for providing materials and laboratory facilities for this research study. Furthermore, the authors extend their appreciation to the Finite Element Simulation Centre of the Rubber Research Institute of Sri Lanka, Rathmalana for facilitating the use of licensed applications of the ABAQUS package for this study.

REFERENCES

ABAQUS G. (2014). *Abaqus 6.14 User's Guide*. Dassault Systemes Simulia Corporation, Providence, RI, USA.

Azizi Y. (2020). Measurement methods of tire/road noise. In: *Automotive Tire Noise and Vibrations* (ed X. Wang), pp. 65–90. Butterworth-Heinemann, Oxford, UK. DOI: https://doi.org/10.1016/b978-0-12-818409-7.00005-2

Chang C.L. & Yang S.H. (2009). Simulation of wheel impact test using finite element method. *Engineering Failure Analysis* **16**(5): 1711–1719. DOI: https://doi.org/10.1016/j.engfailanal.2008.12.010

Dechwayukul C., Kao-ien W., Chetpattananondh K. & Thongruang W. (2010). Measuring service life and evaluating the quality of solid tires. *Sonklanakarin Journal of Science and Technology* **32**(4): 387–390.

Duni E., Toniato G., Saponaro R. & Smeriglio P. (2008). Vehicle fatigue load prediction based on finite element tire/road interaction implemented in an integrated implicit-explicit approach. *Proceedings of the 2008 Abaqus Users' Conference,* 19-22 May. Newport, Rhode Island, USA.

Eindhoven University of Technology. (2021). *Dynamic Mechanical Thermal Analysis – DMAT.* Eindhoven University of Technology. Available at: *https://research.tue.nl/en/equipments/dynamic-mechanical-thermal-analysis*, Accessed 4 April 2021.

Gao Q., Shan Y., Wan X., Feng Q. & Liu X. (2019). 90-degree impact bench test and simulation analysis of automotive steel wheel. *Engineering Failure Analysis* **105**: 143–155. DOI: https://doi.org/10.1016/j.engfailanal.2019.06.097

Han M.J., Lee C.H., Park T.W., Kim Y.S., Shin K.D. & Sim K.S. (2019). Cleat impact analysis of a multi-body quarter vehicle system with finite element models. *International Journal of Mechanical Engineering and Robotics Research* **8**(6): 880–884. DOI: https://doi.org/10.18178/ijmerr.8.6.880-884

Han M.J., Lee C.H. & Park T.W. (2020). Vibro-acoustic response in vehicle interior and exterior using multibody dynamic systems due to cleat impacts. *International Journal of Automotive Technology* **21**(3): 591–602. DOI: https://doi.org/10.1007/s12239-020-0056-1

Hills Kerbs Pty Ltd. (2021). *Concrete Kerbing*. Available at *https://www.hillskerbs.com.au/kerbing/concrete-kerbing,* Accessed 1 May 2021.

Kamoulakos A. & Kao B.G. (1998). Transient dynamics of a tire rolling over small obstacles—a finite element approach with PAM-SHOCK. *Tire Science and Technology* **26**(2): 84–108. DOI: https://doi.org/10.2346/1.2135964

Mooney M. (1940). A theory of large elastic deformation. *Journal of Applied Physics* **11**(9): 582–592.

Ogden R.W. (1972). Large deformation isotropic elasticity on the correlation of theory and experiment for incompressible rubberlike solids. *Proceedings of the Royal Society of London A* **328**: 565–584. DOI: https://doi.org/10.1098/rspa.1972.0096

Ogden R.W. (1973). Large deformation isotropic elasticity—on the correlation of theory and experiment for incompressible rubberlike solids. *Rubber Chemistry and Technology* **46**(2): 398–416.

Neves R.R.V., Micheli G.B. & Alves M. (2010). An experimental and numerical investigation on tyre impact. *International Journal of Impact Engineering* **37**(6): 685–693.

DOI: https://doi.org/10.1016/j.ijimpeng.2009.10.001

Phromjan J. & Suvanjumrat C. (2018a). A suitable constitutive model for solid tire analysis under quasi-static loads using finite element method. *Engineering Journal* **22**(2): 141–155.
DOI: https://doi.org/10.4186/ej.2018.22.2.141

Phromjan J. & Suvanjumrat C. (2018b). Vibration effect of two different tires on baggage towing tractors. *Journal of Mechanical Science and Technology* **32**(4): 1539–1548. DOI: https://doi.org/10.1007/s12206-018-0307-5

Phromjan J. & Suvanjumrat C. (2020). The contact patch analysis of solid tire on drum testing by finite element method. *IOP Conference Series: Materials Science and Engineering* **886**: 012049.
DOI: https://doi.org/10.1088/1757-899x/886/1/012049

Reida J.D., Boesch D.A. & Bielenberg R.W. (2007). Detailed tire modeling for crash applications. *International Journal of Crashworthiness* **12**(5): 521–529.
DOI: https://doi.org/10.1080/13588260701483813

Shiraishi M., Yoshinaga H., Iwasaki N. & Hayashi K. (2000). Making FEM tire model and applying it for durability simulation. *Proceedings of the 6th International LS-Dyna Users Conference 2000.* Detroit, USA.

Suripa U. & Chaikittiratana A. (2008). Finite element stress and strain analysis of a solid tyre. *Journal of Achievements in Materials and Manufacturing Engineering* **31**(2): 576–579.

Suvanjumrat C. & Phromjan J. (2020). The contact patch characterization of various solid tire testing methods by finite element analysis and experiment. *International Journal of GEOMATE* **19**(76): 25–32.
DOI: https://doi.org/10.21660/2020.76.9134

Suvanjumrat C. & Rugsaj R. (2020). The dynamic finite element model of non-pneumatic tire under comfortable riding evaluation. *International Journal of GEOMATE* **19**(76): 62–68.
DOI: https://doi.org/10.21660/2020.76.9135

Yeoh O.H. (1990). Characterization of elastic properties of carbon-black-filled rubber vulcanizates. *Rubber Chemistry and Technology* **63**(5): 792–805.

Yeoh O.H. (1997). Hyperelastic material models for finite element analysis of rubber. *Journal of Natural Rubber Research* **12**(3): 142–153.

Wei C. & Olatunbosun O.A. (2014). Transient dynamic behaviour of finite element tire traversing obstacles with different heights. *Journal of Terramechanics* **56**: 1–16.
DOI: https://doi.org/10.1016/j.jterra.2014.07.001